Applied Catalysis B: Environmental 98 (2010) 229–234

Contents lists available at ScienceDirect

Applied Catalysis B: Environmental

journal homepage: www.elsevier.com/locate/apcatb

# Silver–$TiO_2$ nanocomposites: Synthesis and harmful algae bloom UV-photoelimination

V. Rodríguez-González[a,*], S. Obregón Alfaro[b], L.M. Torres-Martínez[c], Sung-Hun Cho[d], Soo-Wohn Lee[d]

[a] IPICYT, Instituto Potosino de Investigación Científica y Tecnológica, División de Materiales Avanzados, Camino a la Presa San José 2055 Col. Lomas 4a. sección C.P. 78216, San Luis Potosí, S.L.P., Mexico
[b] Universidad Autónoma de Nuevo León, Facultad de Ingeniería Mecánica y Eléctrica, Ciudad Universitaria, C.P. 66451, San Nicolás de los Garza, N.L., Mexico
[c] Universidad Autónoma de Nuevo León, Facultad de Ingeniería Civil, Instituto de Ingeniería Civil, Departamento de Ecomateriales y Energía, Av. Universidad S/N, San Nicolás de los Garza, Nuevo León, C.P. 66451, Mexico
[d] Department of Materials Engineering, Sun Moon University, Galsan-Ri, Tangjung-Myon, Asan Chungnam, 336-708, South Korea

ARTICLE INFO

*Article history:*
Received 27 November 2009
Received in revised form 13 May 2010
Accepted 2 June 2010
Available online 11 June 2010

*Keywords:*
$TiO_2$ sol–gel
Silver nanoparticles
Harmful algae bloom
Silver photodeposition

ABSTRACT

Silver $TiO_2$ nanocomposites were synthesized by two methods: silver UV photodeposition (Ag/P25) and a sol–gel process incorporating silver nitrate during the titanium alkoxide gelling step ($TiO_2$-Ag). The obtained nanocomposites were characterized by means of XRD, $N_2$ adsorption, XPS, and DRS. All the silver-$TiO_2$ semiconductors have anatase as the principal crystalline $TiO_2$ phase and the average band gap was found in the edge of the visible–ultraviolet region (3.26 eV). According to XPS and HAADF-STEM studies, highly dispersed silver nanoparticles were found on the titania surface as Ag°. The photocatalytic effects of the silver $TiO_2$ nanocomposites on the killing of marine algae were examined by using either *Amphidinium carterae* (red tide) or noxious *Tetraselmis suecica* (green tide) as a probe. After 1 h under UV irradiation, both harmful algae were inactivated by the silver nanocomposites. The fatal damages to these microorganisms induced by the $TiO_2$-Ag sol–gel semiconductor occurred faster than those promoted by the Ag/P25 and $TiO_2$ sol–gel isolated supports. In addition to the biocide properties of silver in aqueous medium, the silver nanoparticles acted as electron traps, retarding electron–hole recombination, which enhanced the photocatalytic activity.



## 1. Introduction

The conjunction of different events can modify severely the balance of basin life in sea waters and rivers. Harmful algae and phytoplankton blooms are the principal evidence of coastal eutrophication [1–2]. These events are continuously observed in oceans, rivers and lakes all over the world [3–5]. Red and green tides are well known names of harmful algal bloom (HAB). *Ulva* spp. is mostly responsible for green tides, whereas raphidophyceae and dinoflagellates for the red tide [6–8]. Due to the unexpected increase in the population of microalgae, which are regularly present in the seas and river basins, the color of water turns red or brown. Sometimes, water does not change its color at all, but deadly algae may still be present. Some algal species produce neurotoxins and toxic phytoplankton. They can accumulate in shellfish which feed on algae, which make them poisonous. Toxic phytoplankton is accumulated in the digestive system of fish and filter feeders, which subsequently cause either illnesses or death to consumers. Other kinds of algae may kill sea life by reducing water oxygen levels. In some red tides, thousands of dead fish appear on beaches [7]. Some solutions have been proposed to solve these problems, but deactivation of these harmful algae on the short-term scale has not been achieved [8–11]. The pathophysiological properties of titania seem to be a good option to rapidly deactivate them [12–14]. In addition, titanium dioxide modified with silver nanoparticles has been shown to be an excellent material for the inactivation or even the killing of bacteria and fungi [15–21] and for the decomposition of organic contaminants in water [22–27].

The aim of this research is to find an alternative way to deactivate HAB by employing $TiO_2$ semiconductors functionalized with silver nanoparticles. The nanocomposites were prepared by two methods and characterized by means of XRD, $N_2$ physisorption, UV–vis diffuse reflectance, XPS, and HAADF-STEM. The photokilling of *Amphidinium carterae* and *Tetraselmis suecica* was performed to evaluate the nanocomposites.

## 2. Experimental

### 2.1. Preparation of silver-loaded photocatalysts

The silver nanocomposites were synthesized by two methods: a sol–gel process and photochemical impregnation. First, an appro-

* Corresponding author. Tel.: +52 (444) 8342000x7295; fax: +52 (444) 8342010.
*E-mail address:* vicente.rdz@ipicyt.edu.mx (V. Rodríguez-González).

0926-3373/$ – see front matter © 2010 Elsevier B.V. All rights reserved.
doi:10.1016/j.apcatb.2010.06.001

priated amount of 0.4771 g of silver nitrate (Samchun, 99.8%) to obtain 1.0 wt% Ag, was dissolved in 27.6 mL of bidistilled water and placed in an ultrasonic bath for 5 min to assure the complete disaggregation of the silver precursor. The sol–gel-silver–titania nanocomposite was prepared by adding dropwise 130.36 g of titanium n-butoxide (Sigma–Aldrich, 97%), 53.2 mL n-butanol and the silver solution to a 53.2 mL butanol–27.6 mL water solution contained in a 4-neck round bottom flask (1 L) equipped with magnetic stirrer and thermometer. The alkoxide/n-butanol/water molar ratio was 1/3/8 and the final amount of silver was 1 wt%. Then the reactant solution was maintained in the dark under constant stirring for 4 h at 80 °C. The gelled product was aged for 72 h. The solvents and unreacted precursors were removed in a vacuum evaporator at 80 °C, dried overnight under vacuum at 100 °C, and finally calcined at 450 °C for 4 h. A reference $TiO_2$ sol–gel sample ($TiO_2$-SG) was prepared according to the method described above, but without the addition of silver.

For photochemical impregnation, titanium dioxide powder (P25, Degussa) was the titania support. The 29.7 g of $TiO_2$ powder was added to 1 L of an aqueous solution containing 0.472 g $AgNO_3$, previously magnetically stirred for 15 min, and then put in an ultrasonic bath for 5 min to assure the complete disaggregation of agglomerated particles. Then, the slurry was maintained for 1 h under continuous magnetic stirring to achieve adsorption equilibrium of the $Ag^+$ ions on the $TiO_2$ surface. Afterwards, the slurry was irradiated with two 20 W UV A-type lamps (Black light lamp-BL, Sankyo Denky, Japan) for 2 h. The fresh preparation was stabilized in a vacuum rotary evaporator at 80 °C for 4 h, dried overnight in the dark at 100 °C in a vacuum oven, and finally stored in a vessel that was not exposed to light. The silver nanocomposites prepared by sol–gel were identified as $TiO_2$-Ag and Ag/P25 for the silver nanocomposites which were prepared by photochemical impregnation.

### 2.2. Characterization of nanocomposites

X-ray powder diffraction (XRD) measurements (Brucker D8 Advanced diffractometer, Cu Kα radiation, from 10° to 70° 2$\theta$) were used to identify the crystalline phases of the silver-modified $TiO_2$ and silver-photoimpregnated semiconductors. The crystallite sizes were calculated from the peak width using the Scherrer equation: $D = k\lambda/\beta\cos\theta$, where $D$ is the crystallite size, $k$ is a constant (in this study $k = 0.89$), λ is the CuKα X-ray wavelength (1.5406 Å) and $\beta$ is the half-width of the peak at 2$\theta$. The specific surface areas (BET method) and mean pore size diameters (BJH method) were determined in samples that were degassed for 12 h at 300 °C from the nitrogen adsorption–desorption isotherms that were obtained with an Autosorb 3B apparatus (Quantachrome). The determination of the silver oxidation state was performed by X-ray photoelectron spectroscopy (XPS) with an XPS, ESCA-3200 Shimadzu electron spectrometer equipped with a hemispherical analyzing system. The spectrometer was operated in a constant pass energy mode with a monochromatized MgKα ($h\nu$ = 1253.6 eV) source. The X-ray source was operated at 30 mA and 8 kV. The intensity of the peaks was estimated by integrating each peak after subtracting an S-shaped background and fitting the experimental peaks to a combination of Lorentzian/Gaussian lines of variable proportions by using the ORIGIN LAB 7 software. The binding energies (BE) were referenced to the C 1s peak, whose BE was fixed at 284.6 eV (adventitious carbon). The UV–vis diffuse reflectance spectra were obtained with a Varian Cary 100 spectrometer with a $BaSO_4$ coated integration sphere. The samples were placed in a Teflon cell (thickness of ~2 mm) to measure the remission function $F(R\infty)$. HAADF-STEM micrographs were obtained with a transmission electron microscope JEOL 2200 FS, with spherical aberration corrector in the scanning transmission electron microscope (STEM) mode. The sample was dispersed in methanol and then one drop was placed on a lacy carbon support cupper grid. The images were acquired in STEM mode using a high angle annular dark field (HAADF) detector to distinguish between heavy and light atoms.

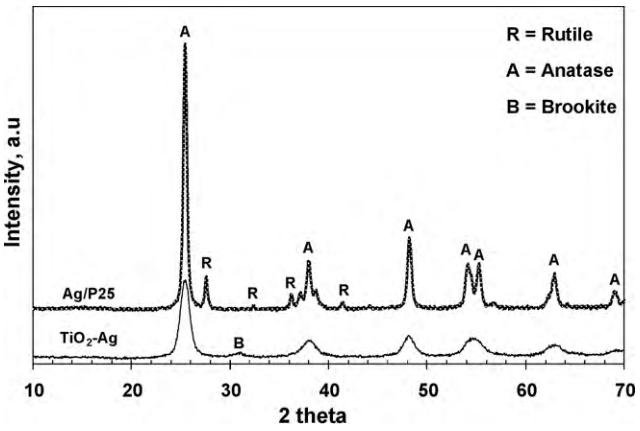


**Fig. 1.** XRD patterns for the sol–gel silver-doped titania and silver photodeposed on P25 semiconductors annealed at 450 °C.

### 2.3. Photoinactivation of harmful algae

In a glass beaker, 100 mg of photocatalyst were suspended with 200 mL of a dispersion of either *A. carterae* (red tide) in sea water whose initial concentration was $100 \pm 10 \times 10^3$ cells $mL^{-1}$ (Natural Live Plankton Co., Ltd., 99.9%) or *T. suecica* (green tide) $250 \pm 20 \times 10^3$ cells $mL^{-1}$ (NLP Co., Ltd., 99.9%). Then, the suspension was magnetically stirred and exposed to UV irradiation (345–400 nm) using two 20 W A-type UV lamps (Black light lamp-BL, Sankyo Denky, Japan). The experiments were performed at room temperature. At given irradiation intervals, 100 μL of the suspension were collected and analyzed to obtain the counting cell concentration with a hemacytometer under a Motic-BA200 optical microscope. About 30–100 cells were counted once and the counting was carried out three times for each sample. For comparative purposes, photokilling experiments were also performed using $TiO_2$-SG Degussa P25. All the photokilling experiments were repeated at least twice. Estimated counting errors did not exceed 5.0%. Nutritive water (Natural Live Plankton Co. Ltd.) was added to the system after incubation at 25 °C for 72 h to confirm that the damage to the algae is irreversible. Afterwards, the suspension was analyzed for the counting cell concentration, but no living cells were detected.

## 3. Results and discussion

### 3.1. Characterization of the silver–$TiO_2$ nanocomposites

The XRD patterns for the silver $TiO_2$-doped-SG and $TiO_2$ P25 silver photodeposited semiconductors are showed in Fig. 1. For the $TiO_2$-Ag sol–gel semiconductor, the $TiO_2$ anatase crystalline phase (JCPDS 21-1272) also showed by a small peak at 30.83 of 2$\theta$, which may be assigned to brookite (JCPDS 76-1934), while for the Ag/P25 photodeposited semiconductor showed the typical anatase and rutile (JCPDS 21-1276) $TiO_2$ crystalline phases. These results illustrate that brookite–anatase phases are present in the $TiO_2$ sol–gel sample, the semiconductors prepared by silver photodeposition on Degussa P25 showed that the anatase and rutile phases were preserved after the incorporation of silver. The anatase crystallite size (25.4 of 2$\theta$) in the samples was calculated by using the Scherrer equation (Table 1). For the silver on commercial $TiO_2$ P25 this is of 25 nm, while for the sol–gel sample it is 8 nm. It seems

**Table 1**
Specific surface area, mean pore size diameter and anatase crystallite size for the silver-supported semiconductors.

| Material | BET ($m^2\ g^{-1}$) | Mean pore size (nm) | Anatase crystallite size[a] (nm) | Eg (eV) |
|---|---|---|---|---|
| $TiO_2$P25 | 56 | – | 29 | 3.50 |
| $TiO_2$-SG | 66 | 14 | 12 | 3.44 |
| $TiO_2$-Ag | 130 | 7 | 8 | 3.26 |
| Ag/P25 | 52 | – | 25 | 3.49 |

[a] From XRD.

that the incorporation of silver into the titanium butoxide gelling solution inhibits the crystal growth in the sol–gel samples [24]. Characterization of the photophysical properties was performed by UV–vis diffuse reflectance spectroscopy. The UV–vis spectra for the silver promoted semiconductors are shown in Fig. 2. The diffuse reflectance spectra was plotted using the Kubelka–Munk function: $F(R) = (1-R)^2/2R$ versus wavelength. The Eg was then calculated from the modified plot of the Kubelka–Munk function, $F(R)$ versus Energy (eV), see Fig. 2. The diffuse reflectance UV–vis spectra of the P25 sample shows an absorption band ca. 350 nm, which is shifted to around 360 nm in the Ag/P25 and bare $TiO_2$-SG semiconductors. For the $TiO_2$-Ag sol–gel sample, the absorption band was found at around 385 nm. The absence of the surface plasmon resonance band in the Ag-supported semiconductors indicates that in such semiconductors the silver particles are highly dispersed on the surface or incorporated into the $TiO_2$ framework. In Table 1, the band gap energies (Eg) for the various semiconductors are reported. It can be seen that the Eg energies found for the supports are higher than those obtained with the sol–gel silver-supported semiconductor. For instance, the estimated band gap for the $TiO_2$-Ag sol–gel semiconductor is 3.26 eV, and 3.46 eV for Ag/P25, but 3.49 and 3.52 eV for the bare $TiO_2$ sol–gel and commercial titania P25, respectively. The effect of silver incorporated on the extended value of Eg to the visible was attributed to the electron acceptor character of the surface silver nanoparticles as is illustrated in the Kubelka–Munk spectra, Fig. 2. The silver particles anchored on the surface of the $TiO_2$-Ag sol–gel accepted the photons generated by the UV–vis spectrophotometer, which resulted in the low intensity of the $F(R)$ function, extending the photon absorption into the visible region edge [20].

The specific surface areas for the various supports and silver-supported semiconductors are listed in Table 1. For the $TiO_2$-SG and $TiO_2$ P25 reference materials, the BET areas are 66 and 56 $m^2/g$, respectively; for the $TiO_2$-Ag sol–gel, and Ag/P25, the BET areas are 130 $m^2/g$ and 52 $m^2/g$, respectively. The superior specific surface area in the sol–gel silver semiconductor undoubtedly is the product of co-gelling of titanium alkoxide with silver nitrate under

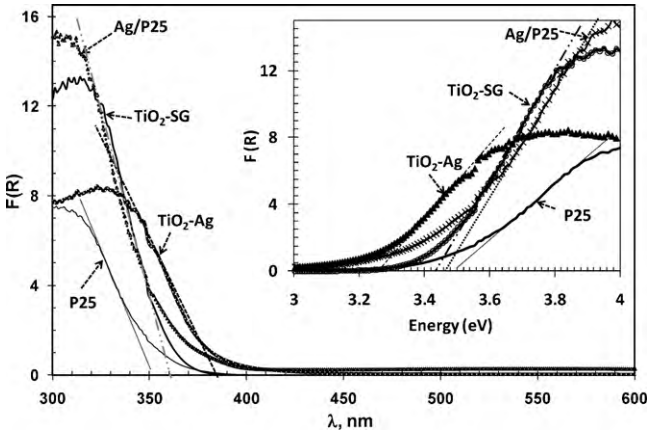


**Fig. 2.** DRS spectra for different silver-$TiO_2$ and $TiO_2$ nanocomposites.

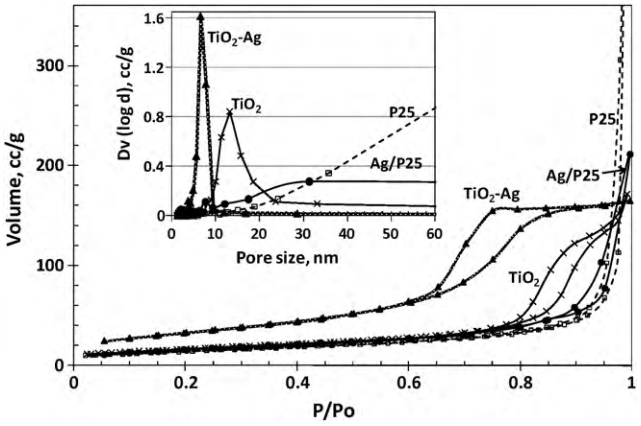


**Fig. 3.** Absorption–desorption isotherms and pore size distributions for sol–gel and photodeposited silver semiconductors.

controlled hydrolysis conditions. This method produces semiconductors with different textural properties from those of reference commercial titania. The nitrogen adsorption–desorption isotherms are presented in Fig. 3, where the classical hysteresis loop for mesoporous materials can be seen in the sol–gel $TiO_2$-Ag. The mean pore size diameters for both silver-supported semiconductors were calculated and the corresponding distributions are also shown in Fig. 3. The textural differences of the silver semiconductors are clearly seen on the absorption–desorption isotherms, where a shift to a lower partial pressure distribution was produced in the sol–gel material. This increase in the specific surface area from 66 to 130 $m^2/g$ with the silver semiconductor may be explained by the small pore size diameter of the sol–gel silver sample, which may be induced by the presence of silver species during the gelling step. The observed pore size diameter was 7 nm in the $TiO_2$-Ag sol–gel sample. Homogenous mesoporous materials were obtained in the sol–gel materials. The macroporous texture of the commercial titania P25 was preserved after the silver photodeposition.

The XPS studies of the semiconductors show that the Ti 2p XPS and O 1s XPS peaks have binding energies of 459.5 and 530.6 eV, respectively. The binding energies for Ti and O coincide fairly well with that reported in the literature for $TiO_2$ semiconductors [28]. This suggests that silver incorporation did not affect the XPS peaks of these elements [23,27] in our samples. The XPS analysis was carried out to identify the surface oxidation states of the silver particles incorporated either by the sol–gel process or by photodeposited silver on the titania semiconductors. In Fig. 4, the raw XPS spectra for both silver semiconductors and bare $TiO_2$-SG are shown. The Ag 3d peaks appear at a binding energy of 368.5 eV ($3d_{5/2}$) and the splitting of the 3d doublet ($3d_{3/2}$) is approximately at 6.0 eV. These binding energies indicate that a large amount of reduced silver particles ($Ag^\circ$) exist on the $TiO_2$ support surface [23,24]. The intensity of the silver XPS spectra for the Ag/$TiO_2$ semiconductor shows greater intensity than $TiO_2$-Ag sol–gel semiconductor. This difference may be related to the silver dispersion on the surface of $TiO_2$. Intensity differences were quantified by using the full width at half maximum (FWHM) value of Ag/Ti ratio. Ag/P25 has a Ag/Ti ratio of 0.8571 and $TiO_2$-Ag sol–gel has a Ag/Ti ratio of 1.25. When silver was incorporated by sol–gel process, the silver particles are more dispersed. The deconvoluted XPS spectra in the Ag 3d region for the Ag/P25 is shown in Fig. 5. The deconvoluted spectra show the Ag $3d_{5/2}$ peak at a binding energy of 368.5 eV, while for the Ag $3d_{3/2}$, the peak is placed at a binding energy of 374.5 eV. The Ag $3d_{5/2}$ and Ag $3d_{3/2}$ binding energies for $Ag^\circ$ have been reported ca. 368.2 and 374.2 eV, respectively [23,24]. Two additional peaks were observed at 369.4 and 375.4 eV. On the other hand, in Fig. 6, for the $TiO_2$-Ag semiconductor, the $3d_{5/2}$ and $3d_{3/2}$ peaks for $Ag^\circ$

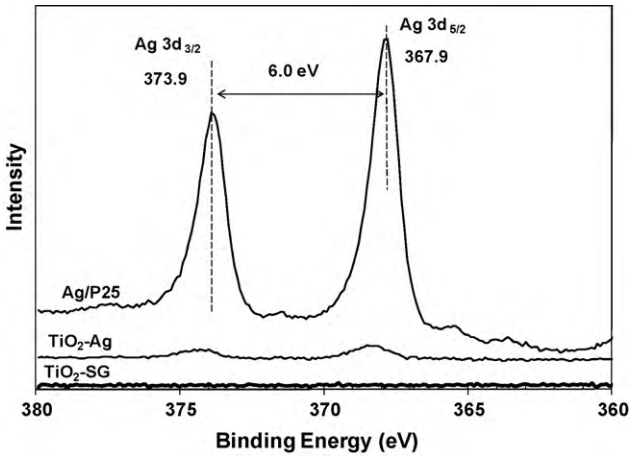


**Fig. 4.** Ag 3d XPS spectra for the silver-supported semiconductors and support.

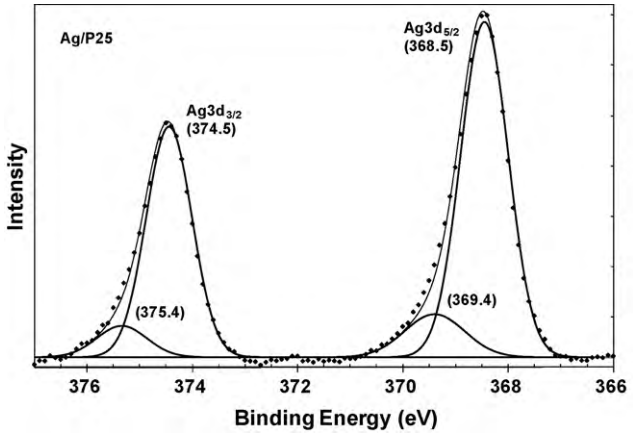


**Fig. 5.** Deconvoluted XPS spectra of Ag/P25.

can also be seen at binding energies of 368.6 and 374.6 eV, respectively; two additional peaks were also found at 367 and 374 eV, which could be assigned to AgO nanoclusters [23]. Therefore, we can say that in both silver semiconductors (prepared by different methods) stabilized reduced silver particles are mainly observed. In addition, it is possible to suggest that the silver particles on the titania surface have different interactions with the support. In the case of the photodeposition of silver nitrate onto the titania Degussa P25, no evidence of anchorage or chemical bonds of may be $Ag^{\circ}$ or AgO to $Ti^{4+}$ or O was found. Otherwise, nanometric metallic silver particles are possibly highly dispersed on the titania P25 because no SPR band was present in the UV–vis spectroscopy. The high intensity of the 3d XPS peaks for this photoimpregnated semiconductor (Fig. 4) in comparison with the XPS peaks for the doped semiconductor confirms that the particles are deposited on the surface without chemical bonding to titania surface. The peaks found by the deconvolution (Fig. 5) show 3d Ag peaks at 368.5 and 374.5 eV, which are typical of $Ag^{\circ}$, while the other 3d Ag peaks at 375.4 and 369.4 eV could suggest the presence silver particles of different size. As for the incorporation of silver nitrate during the titanium alkoxide gelling step, possible evidence of anchored or immobilized silver particles by surface chemical bond is given by the 3d Ag XPS spectra, with peaks at 367 and 374 eV, which are normally assigned to the AgO state. This may imply that some particles are anchored to the external surface Ti–O bond. A remarkable decrease of the Ag 3d XPS peaks was observed on the $TiO_2$-Ag. Hence these results suggest that mutual interaction between Ag and $TiO_2$ are preferentially with superficial oxygen species. Thus, some $Ag^{+}$ species are probably incorporated into the superficial titania framework. The shift observed in the Ag 3d peak positions of XPS spectra can be attributed to a decrease in silver particle size. Generally considering, a normal energy resolution/error of ±0.1 eV in the binding energy scale, some examples concerning Ag XPS size-sensitivity was reported on silver supported on various substrates such as carbon, HOPG, quartz and $TiO_2$ [29–31], This size dependent change observed in the XPS spectra of the silver–$TiO_2$ nanocompos-

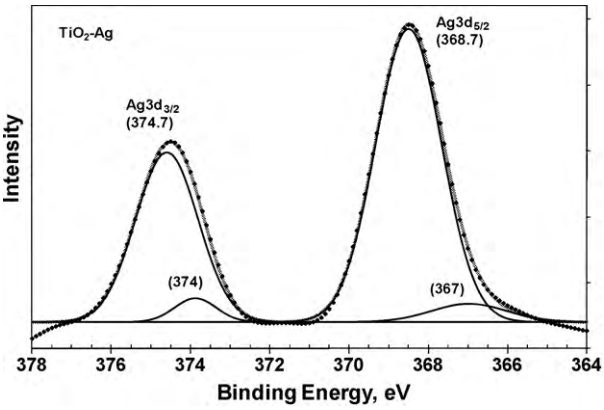


**Fig. 6.** Deconvoluted XPS spectra of Ag-$TiO_2$.

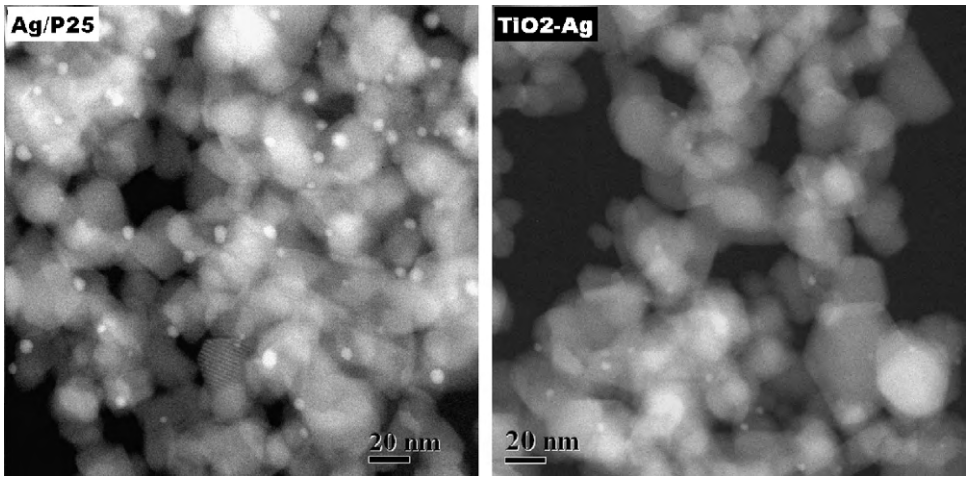


**Fig. 7.** STEM Z contrast images for the Ag/P25 and $TiO_2$-Ag sol–gel semiconductors.

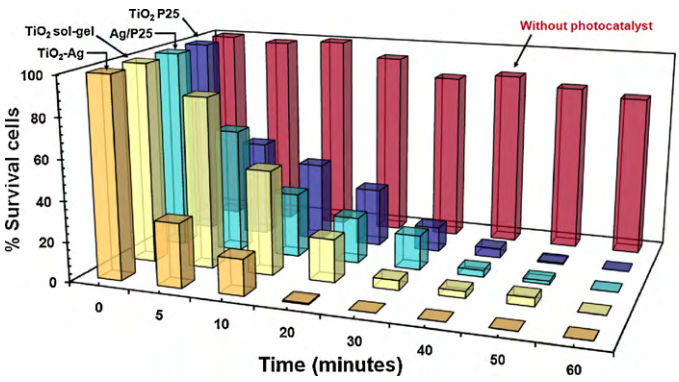


**Fig. 8.** Survival fraction of *Tetraselmis suecica* (green tide) as a function of UV irradiation time.

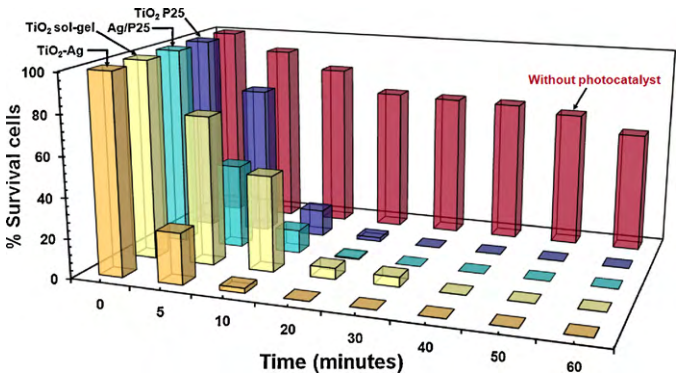


**Fig. 9.** Survival fraction of *Amphidium carterae* (red tide) as a function of UV irradiation time.

ites influences the electronic structure and optical properties of Ag nanoparticles incorporated into the $TiO_2$. STEM studies were performed to estimate particle size effects on the XPS analysis induced by the preparation method. The HAADF-STEM images (Fig. 7) show quasi-spherical silver nanoparticles deposited over the $TiO_2$ surface. In the HAADF-STEM mode, silver nanoparticles with mean size of 4.5 nm can be seen (Fig. 7a) for the Ag/P25 nanocomposite. The mean particle size of the silver nanoparticles incorporated by sol–gel method was around 2.0 nm. These results are in good agreement with the additional peaks observed in the deconvoluted XPS spectra. In the photodeposited silver $TiO_2$-P25 semiconductor, the additional peaks can be related to a high concentration of silver nanoparticles, and the HAADF-STEM images show some particles around 8 nm in diameter. In the case of the deconvoluted XPS spectrum of silver $TiO_2$ sol–gel semiconductor, the additional peaks can be attributed to the decrease of silver nanoparticles size to as small as 1 nm, as seen in the HAADF-STEM image (Fig. 7b).

### 3.2. Photoinactivation of harmful algae

The photocatalytic activities of the semiconductors were evaluated by the UV inactivation of harmful algae bloom, which are responsible for the damage of life in sea. The photokilling properties were investigated by means of two species of marine algae: *A. carterae* (red tide) and noxious *T. suecica* (green tide). The reduction of the number of living cells with irradiation time was used for evaluating the photocatalytic effects of the semiconductors. Fig. 8 shows the green tide inactivation ratio as a function of time for four semiconductors. The test system without semiconductor showed very weak inactivation activities, suggesting that the UV irradiation had no influence on the fatal damage of marine algae. Dark tests of the silver nanocomposites were developed to check the biocide capability of silver in absence of UV light. Under these conditions, the differences in biocide capability of silver nanoparticles were negligible. Silver biocide capability for killing red tide was 18% of survival cells and for green tide were 10% of survival cells.

Total deactivation of green tide was attained by the $TiO_2$-Ag sol–gel semiconductor after 30 min; with the Ag/P25, $TiO_2$ P25 and $TiO_2$-SG semiconductors, total killing was attained after 60 min. The Ag/P25 and $TiO_2$-P25 semiconductors showed faster photokilling compared with the sol–gel $TiO_2$ reference. Nevertheless, the silver sol–gel semiconductors $TiO_2$-Ag attained the best photokilling. In Fig. 9, the red tide killing ratio as a function of time for the four evaluated semiconductors is presented. The photokilling test without the presence of a semiconductor also presented a negligible killing activity. The total elimination of red tide was attained in just 20 min by $TiO_2$-Ag semiconductor. Ag/P25 and $TiO_2$ P25 semiconductors achieved total inactivation in 30 min. Finally, the sol–gel support reached total elimination in 40 min. In general, the silver sol–gel semiconductor presented the best photokilling behavior, suggesting that silver enhanced the marine tide photokilling, and also that red tide was easier to kill than green tide. Direct contact between harmful algae and semiconductor powders is necessary to induce fatal damages on the body surface [12]. The body size of marine microalgae is ca. 120 μm long and ca. 50 μm wide. The semiconductor surrounds and immobilizes the algae, which increases the damage due to its photoactive properties [12]. During the photokilling process, the microorganism is first covered until it is immobilized and damaged by photons generated by the semiconductor. After 5 min the algae body is deformed and starts to fragment until it is totally destroyed. The roles of silver particles consist in capturing electrons and inhibiting electron recombination. In addition, the biocide properties of silver enhance the fatal damage to the algae [22]. The photokilling effects are enhanced on the sol–gel silver semiconductors because of high specific surface area, the $TiO_2$ anatase crystalline phase of the supports and the nanometric silver particles size <5 nm. The body size of both algae must be considered; According to the NLP Co. Ltd. (Korea) certificate, *A. carterae* (NPL-14) has a round or oval flagellates morphology of 5–8 μm width by 10–20 μm of length in contrast with *T. suecica* (NPL-13) that is mostly a round flagellates, 3–8 μm wide and 7–14 μm long. Perhaps the difference in size and morphology explains why Tetraselmis plankton is easier to be covered and faster to be killed.

The properties of incorporating silver nanoparticles either by sol–gel or photochemical deposition allowed stabilization of the highly dispersed $Ag^{\circ}$ nanoparticles because of the continuing UV irradiation during the photokilling process. Under UV irradiation the lixiviation of silver to the solution may become negligible [20]. ICP analysis detected 1.7435 ppm of silver after 1 h of stirring 100 mg of Ag/P25 under UV light and 0.4065 ppm in the case of $TiO_2$-Ag sol–gel semiconductor. Sol–gel preparation results in greater stability than photodeposited material which may improve the photochemical process.

The mechanistic insight of the photokilling action of these materials to the algal cells is still unclear due to the various classes of algal species and will be the focus of further studies. It is not possible to separate the toxic effect of silver of the biocide and photochemical properties of silver nanoparticles, because it is a synergy effect. Silver toxicity possible alters the membranes of the cells while the photoactivity of silver–titania nanocomposite fragments the cytoplasm, as the biocide properties inhibit the growth of unicellular algal. Silver incorporation attainable changes the surface characteristics of $TiO_2$, yielding greater surface area with photoactive and biocide $Ag^{\circ}$ sites highly dispersed on surface. Thus, the enhancement in the photoelimination is not due exclusively to a greater electron–hole separation and extended visible Eg excitation, but is also liable due to the biocide role of silver in titania nanocomposites

[20]. Furthermore, silver nanoparticles exposure under UV-light, at lixiviation concentration, does not induce morphological damage. I was reported that exposure of silver nanoparticles (<30 nm) induces morphological malformations to fish cells and gram positive bacteria in long exposures of more than seven days [32,33].

The possible applications of these materials may be helpful in the stress of HBA where the dinoflagellate species are the main phytoplankton population. The materials have to act just before HAB begis to produce toxins that kill fish and make shellfish dangerous to eat; avoiding the damage of other benefit phytoplankton.

## 4. Conclusions

The preparation of silver–$TiO_2$ nanocomposites by the sol–gel method allows the formation of solids with important properties that induce the following effects on the silver nanoparticles deposited on them: (i) high concentration of silver in the reduced state ($Ag^{\circ}$) and (ii) the silver nanoparticles extend the Eg band gap to lower energy. The particular properties of the $TiO_2$-Ag materials show that these solids are promising materials that can successfully photokill harmful marine algae in 30 min. The function of the silver nanoparticles was exhibited by using a silver photodeposited on commercial $TiO_2$ support. The silver nanoparticles may act as electron traps, inhibiting the electron recombination, which enhanced photocatalytic activity. The biocide properties of silver in an aqueous medium probably also play an important role.

## Acknowledgements

The authors thank Professor R. Gómez for his comments and technical support provided to this work through the "Programa de Apoyo Complementario para la Consolidación Institucional", CONACYT 2007. This work was also supported by the Korea Research Foundation Grant (Bilateral Cooperative Research between Korea and México, 2008). VRG thank the Laboratorio Nacional de Nanotecnología located at CIMAV Chihuahua Mexico for STEM results.

## References

[1] Theodore J. Smayda, Harmful Algae 8 (2008) 140–151.
[2] S. Mohr, M. Feibicke, R. Berghahn, R. Schmiediche, R. Schmidt, Environ. Pollut. 152 (2008) 530–542.
[3] B. Kirkpatrick, L.E. Fleming, D. Squicciarini, L.C. Backer, R. Clark, W. Abraham, J. Benson, Y.S. Cheng, D. Johnson, R. Pierce, J. Zaias, G.D. Bossart, D.G. Baden, Harmful Algae 3 (2004) 99–115.
[4] L.U. Dou-ding, J. Goebel, Chin. J. Oceanol. Limnol. 19 (2001) 337–344.
[5] K. Kohata, M. Watanabe, K. Yamanaka, T. Ioriya, T. Kimura, Water Res. 31 (1997) 2269–2277.
[6] V. Evangelista, L. Barsanti, A.M. Frassanito, V. Passarelli, P. Gualtieri (Eds.), Algal Toxins: Nature, Occurrence, Effect and Detection, 1st ed., Springer Science, The Netherlands, 2008.
[7] M. Merceron, V. Antoine, I. Auby, P. Morand, Sci. Total Environ. 384 (2007) 293–305.
[8] R.G. Zepp, P.F. Schlotzhauer, Environ. Sci. Technol. 17 (1983) 462–468.
[9] K.Y. Yoon, J.H. Byeon, C.W. Park, J. Hwang, Environ. Sci. Technol. 42 (2008) 1251–1255.
[10] T. Matsunaga, R. Tomoda, T. Nakajima, H. Wake, FEMS Microbiol. Lett. 29 (1985) 211–214.
[11] J. Dwyer, P. Lant, Biochem. Eng. J. 42 (2008) 47–54.
[12] S. Matsuo, Y. Anraku, S. Yamada, T. Honjo, T. Matsuo, H. Wakita, J. Environ. Sci. Health A 36 (2001) 1419–1425.
[13] Y. Oshida, Bioscience and Bioengineering of Titanium Materials, 1st ed., Elsevier Science Ltd., The Netherlands, 2007.
[14] T.H. Kim, S.W. Lee, H. Chen, H.Y. Cho, Mater. Sci. Forum 510–511 (2006) 70–73.
[15] J.J. Song, S.H. Cho, S.W. Lee, T.H. Kim, Y. Hayashi, Mater. Sci. Forum 544–545 (2007) 135–138.
[16] D. Mitoraj, A. Jaczyk, M. Strus, H. Kisch, G. Stochel, P.B. Heczko, W. Macyk, Photochem. Photobiol. Sci. 6 (2007) 642–648.
[17] D.M.A. Alrousan, P.S.M. Dunlop, T.A. McMurray, J.A. Byrne, Water Res. 43 (2009) 47–54.
[18] V.K. Sharma, R.A. Yngard, Y. Lin, Adv. Colloid Interface Sci. 145 (2009) 83–96.
[19] D. Mitoraj, Photochem. Photobiol. Sci. 6 (2007) 642–648.
[20] R. van Grieken, J. Marugán, C. Sordo, P. Martínez, C. Pablos, Appl. Catal. B: Environ. 93 (2009) 112–118.
[21] A. Kubacka, M. Ferrer, A. Martínez-Arias, M. Fernández-García, Appl. Catal. B: Environ. 84 (2008) 87–93.
[22] S.A. Amin, Power Technol. 196 (2009) 241–245.
[23] X.G. Hou, M.D. Huang, X.L. Wu, A.D. Liu, Chem. Eng. J. 146 (2009) 42–48.
[24] J. Yu, J. Xiong, B. Cheng, S. Liu, Appl. Catal. B: Environ. 60 (2005) 211–221.
[25] A.R. Malagutti, H.A.J.L. Mourao, J.R. Garbin, C. Ribeiro, Appl. Catal. B: Environ. 90 (2009) 205–212.
[26] H. Czili, A. Horváth, Appl. Catal. B: Environ. 89 (2009) 342–348.
[27] Y. Liu, X. Wang, F. Yang, X. Yang, Micropor. Mesopor. Mater. 114 (2008) 431–439.
[28] P. Stefanov, M. Shipochka, P. Stefchev, Z. Raicheva, V. Lazarova, L. Spassov, J. Phys.: Conf. Ser. 100 (2008) 012039.
[29] B. Balamurugan, T. Maruyama, J. Appl. Phys. 102 (2007) 034306.
[30] H. Zhang, Q. Fu, Y. Yao, Z. Zhang, T. Ma, D. Tan, X. Bao, Langmuir 24 (2008) 10874–10878.
[31] V. Iliev, D. Tomova, L. Bilyarska, A. Eliyas, L. Petrov, Appl. Catal. B 63 (2006) 266–271.
[32] H.V. Tran, L.D. Tran, C.T. Ba, H.D. Vu, T.N. Nguyen, D.G. Pham, P.X. Nguyen, Colloid Surf. A: Phys. 360 (2010) 32–40.
[33] J.P. Wise Sr., B.C. Goodale, S.S. Wise, G.A. Craig, A.F. Pongan, R.B. Walter, W.D. Thompson, A.-K. Ng, A.M. Aboueissa, H. Mitani, M.J. Spalding, Michael D. Mason, Aquat. Toxicol. 97 (2010) 34–41.